Flexible and Extensive Platinum Ion Gel Condensers for Programmable Catalysis

Tzia Ming Onn[1,2], Kyung-Ryul Oh[1,2], Demetra Z. Adrahtas[2], Jimmy K. Soeherman[2], Justin A. Hopkins[1,2], C. Daniel Frisbie[1,2], Paul J. Dauenhauer[1,2*]

[1] Center for Programmable Energy Catalysis (CPEC), University of Minnesota, 421 Washington Ave. SE, Minneapolis, MN, USA 55455.

[2] University of Minnesota, Department of Chemical Engineering & Materials Science, 421 Washington Ave. SE, Minneapolis, MN, USA 55455

* Corresponding author: hauer@umn.edu

Abstract. Catalytic condensers comprised of ion gels separating a metal electrode from a platinum-on-carbon active layer were fabricated and characterized to achieve more powerful, high surface area dynamic heterogeneous catalyst surfaces. Ion gels comprised of PVDF/ $[EMIM]^+[TFSI]^-$ were spin coated as a 3.8 μm film on a Au surface, after which carbon sputtering of a 1.8 nm carbon film and electron-beam evaporation of 2 nm Pt clusters created an active surface exposed to reactant gases. Electronic characterization indicated that most charge condensed within the Pt nanoclusters upon application of a potential bias, with the condenser device achieving a capacitance of ~20 $\mu F/cm^2$ at applied frequencies up to 120 Hz. Maximum charge of ~10^{14} $|e^-|$ cm^{-2} was condensed under stable device conditions at 200 °C on catalytic films with ~10^{15} sites cm^{-2}. Grazing incidence infrared spectroscopy measured carbon monoxide adsorption isobars indicating a change in CO* binding energy of ~16 kJ mol^{-1} over an applied potential bias of only 1.25 V. Condensers were also fabricated on flexible, large area Kapton substrates allowing stacked or tubular form factors that facilitate high volumetric active site densities, ultimately enabling a fast and powerful catalytic condenser that can be fabricated for programmable catalysis applications.

1.0 Introduction. Modulation of charge density in metal or metal oxide catalysts with time allows for the direct control of surface chemistry and the acceleration of reaction rates via programmed perturbations of the catalyst.[1,2] Recently, we described a method for stabilizing positive or negative charges in a catalytic layer within 'catalytic condenser' stack devices that use a high dielectric constant (high-*k*) HfO_2 layer to separate charge between a conductive catalyst-on-graphene electrode from a conductive silicon electrode.[3,4] When positive or negative voltages were applied across the electrodes, electrons either depleted or accumulated in the catalyst/graphene layer as demonstrated with catalysts of amorphous alumina or platinum nanoclusters.[3,4] When depleted of electrons on the catalytic condenser, amorphous alumina, a solid Lewis acid catalyst, became more active in dehydrating alcohols such as isopropyl alcohol.[3] Similarly, condensation of electrons or holes in platinum active sites via negative or positive applied bias, respectively, resulted in reversible modulation of adsorbed carbon monoxide (CO*) binding energies by as much as 0.1 eV in either direction.[4] With its versatility in material selection as a catalyst, the catalytic condenser platform allows for manipulation of reactivity with highly responsive electrons or holes at frequencies in excess of 1000 Hz for different heterogeneous chemistries under both static and dynamic conditions.[5,6,7]

The stacked design of a catalytic condenser relies on a supporting graphene or a conductive carbon film to distribute charge across the device surface with HfO_2 as the insulating dielectric layer. The dielectric constant of HfO_2 typically of 25-30 limits the maximum charge density stabilized on the catalyst/carbon top layer. For a potential of ±10 V applied across a 70 nm thick HfO_2, the maximum amount of charge condensed is approximately 10^{13} $|e^-|$ per cm^2. With metals or metal oxides having catalytic site densities of around 10^{15} per cm^2, only 1% of electrons or holes are stored per catalyst active site; more charge per unit area must be

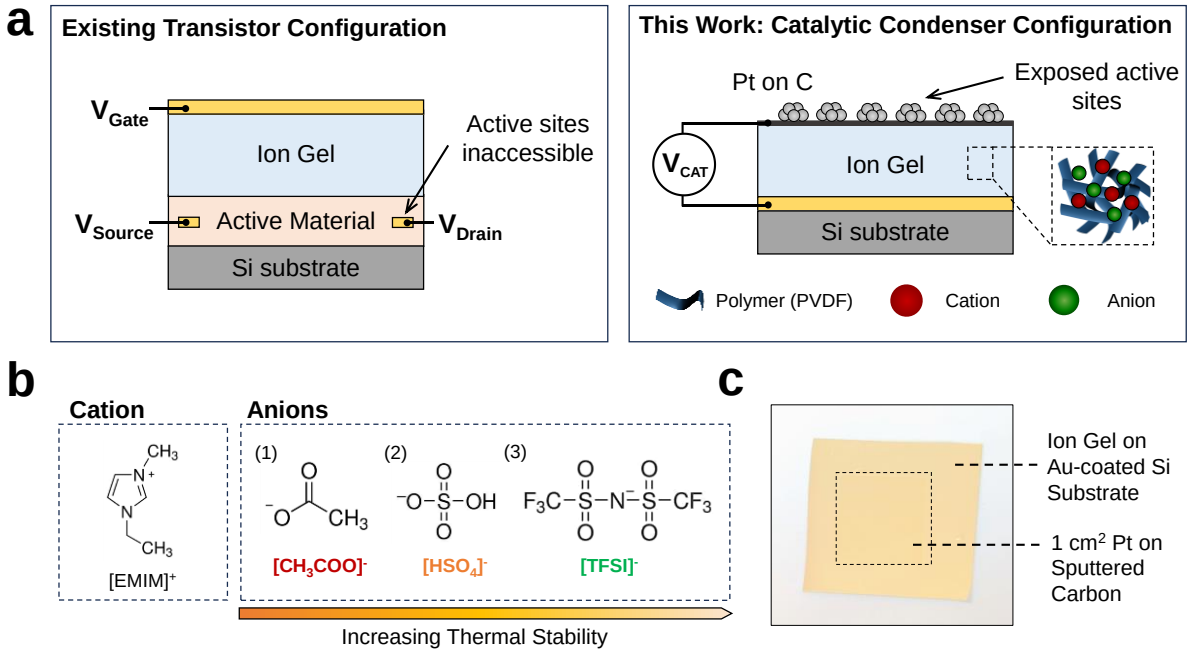

Figure 1. (a) Schematic of an ionic-gated transistor configuration compared to this work's ion gel catalytic condenser configuration with exposed catalytic sites. PVDF is the polymer used to support the ionic liquids. **(b)** Chemical structure of the three ionic liquids explored in this work with $[EMIM]^+$ as the cation and three different anions. In terms of thermal stability, the ion gel based on the anions are in the order: $[TFSI]^- > [HSO_4]^- > [CH_3COO]^-$. **(c)** A photograph of a Pt/ C ion gel catalytic condenser.

stabilized to effectively modulate catalyst active sites for applications involving metals. While higher charge density could be achieved with larger applied bias, higher voltages (up to 20 V) across HfO_2 films increase the likelihood of dielectric breakdown and device failure.

Ion gels are one class of solid-state materials that provide higher capacitance and larger charge condensation beyond high-*k* HfO_2. Prepared as a composite of a supporting polymer infiltrated with the cations and anions of an ionic salt or ionic liquid (IL), ion gels are widely used in electrical and electrochemical processes.[8,9,10,11] These solid polymer electrolytes exhibit high specific capacitance (e.g., C_i of 1 to 10 μF/cm^2 compared to high-*k* HfO_2 of 0.1 μF/cm^2 for ~100 nm films) due to the migration of anions and cations within the gel to the electrodes, resulting in electrical double layer formation within nanometers of the electrolyte/gate electrode interface.[12,13,3] Within the last decade, exploration of different combinations of carbon-based polymers (polymers/copolymers) and ionic liquids has improved the polarization response or switching frequencies of ion gels (from hundreds of hertz to thousands of hertz), increasing mobility of the ions across the polymer-gel network and enabling applications involving faster dynamic operations such as that required for catalytic condensers.[14,15,16]

The high capacitance of ion gels in excess of 1-10 μF/cm^2 enables a higher density of condensed holes/electrons in semiconductors and metals. Moreover, the flexible and stretchable mechanical properties of ion gels have enabled wide applications in batteries, supercapacitors, bioelectronic devices, actuators, electrochromic devices, and more.[17,18,19,20,21] When compared to liquid electrolytes, ion gels are functional at elevated temperatures (>100 °C) owing to their low volatility and chemical/mechanical stability. The versatility of ion gels allows for convenient additive manufacturing processes such as drop casting, spin-coating, aerosol jet printing, ink-jet printing, electrohydrodynamic jet printing, and cut-and-stick lamination.[22,23,24,25] In a typical ion-gel transistor configuration or electrolyte-gated transistor (**Figure 1a**, left), the gel is deposited over the semiconductor channel and metal electrodes; subsequent application of potential bias at the drain/source and gate then induces charge

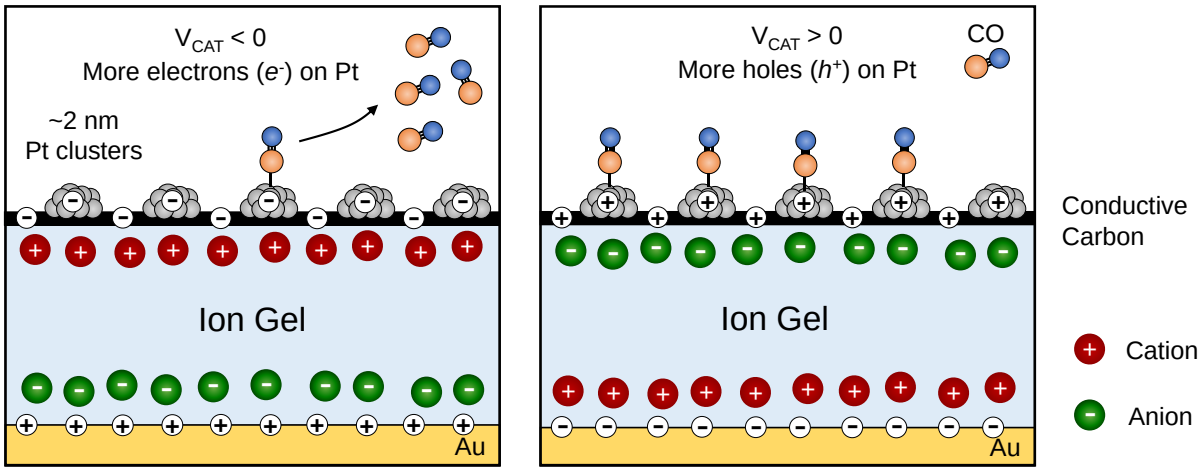

Scheme 1. Pt/ C on an Ion Gel Catalytic Condenser with Negative (Left) and Positive (Right) Charge Condensation, affecting adsorbate CO desorption.

formation in the semiconductor material. However, this configuration, useful for electronic application, has limited utility for catalysis or adsorption applications since the active material is not exposed to an external fluid.

In this study, the recent characterization of thin sputtered carbon films for condenser active layers[26] enabled the implementation of a new ion gel condenser architecture that exposes the active layer to an external fluid (**Figure 1a**, right). Small Pt nanoclusters (~2 nm thick) were dispersed over a continuous and conductive thin (~2 nm) carbon layer that was separated in the condenser from a bottom Au electrode by an ion gel dielectric layer. The ion gel of interest was synthesized from the gelation of the polymer polyvinylidene difluoride (PVDF) and the ionic liquid 1-ethyl-3-methylimidazolium bis(trifluoromethylsulfonyl) imide ($[EMIM]^+[TFSI]^-$), while two other ion gels investigated here differed only in the anionic component of the ionic liquid, namely hydrogen sulfate $[HSO_4]^-$ and acetate $[CH_3COO]^-$ anions. The long-term thermal stabilities of these gels were assessed for their use in thermal catalytic applications, with $[EMIM]^+[TFSI]^-$ being the most stable for catalytic operations over 48 h at 200 °C. When subjected to negative potential biases (V_{CAT} < 0) as shown in **Scheme 1**, electrons accumulating in the platinum/carbon reduced the binding energy of an adsorbate such as carbon monoxide. Likewise, positive bias (V_{CAT} > 0) depleted electrons in the platinum/carbon and increased the adsorbate binding energy. The physical and electronic characteristics of this platinum/carbon ion gel condenser were characterized to demonstrate a tunable metal surface with significant charge condensation on the platinum sites nearly two orders of magnitude greater than earlier HfO_2 devices. Additionally, printing or coating of ion gels on a flexible substrate will allow for roll-to-roll manufacturing of condensers to achieve surface areas required for catalytic or separation applications.

2.0 Results and Discussion. The fabrication of the Pt/ C/ Ion gel/ Au/ Si catalytic condenser, as depicted in **Scheme 1** and **Figure 1**, is described in full detail in the Methods Section and the Supporting Information. Starting with a silicon wafer substrate (~2 cm^2), layers of Au on Ti were first deposited by electron beam deposition. Ion gel, prepared by the gelation of the polymer polyvinylidene difluoride (PVDF) and 1-ethyl-3-methylimidazolium or $[EMIM]^+$-based ionic liquid, was then spin coated on top of the Au layer followed by overnight baking in vacuum (70 °C). The ion gel thickness, as measured by a profilometer, decreased with increasing revolutions per minute, and the selected thickness of 3.8 μm was achieved at 4500 rpm for one minute. The primary ionic liquid component of interest was $[EMIM]^+[TFSI]^-$, and gels of it were compared with two other ion gels made from similar ionic liquids with differing anionic components. Then, a ~1 cm^2 conductive carbon layer (thickness ~2 nm) was sputtered with the assistance of a shadow-mask on top of the ion gel layer. Attempts to grow Pt or Au by electron beam deposition on the ion gel without

the carbon film were not successful, despite a lower deposition power setting and a metal growth rate of only 0.01 Å/sec. Similar to graphene, which was used in previous catalytic condenser devices,[3,4] the sputtered conductive carbon layer has been shown to have sp^2 characteristics, providing a conductive sheet for charge distribution across the surface of the gel while itself having low capacitance. Finally, 1 nm Pt was deposited on the carbon by electron beam evaporation of a pure Pt source followed by reduction in flowing H_2 at 150 °C for an hour which resulted in a ~2 nm Pt nanocluster. The resulting ion gel catalytic condenser is shown in **Figure 1** and features exposed Pt/ C active sites available for molecules to interact with the surface for catalytic applications.

With Pt/ C successfully deposited on top of the ion gel, the catalytic condenser structure was confirmed with SEM and elemental mapping as shown in Figure S3, which demonstrated that both Pt/ C and the ion gel-relevant signals such as F, S, and N corresponding to the ion gel PVDF/ $[EMIM]^+[TFSI]^-$ were evenly distributed across the condenser surface with no large agglomerate formations or significant surface defects. Finally, XPS measurements in Figure S4 also confirmed the elemental presence of Pt, C, and the ion gel components of F, S, and N of the condenser device.

Thermal Stability of Ion Gels: Transient and Isothermal Measurements. The short-term and long-term structural, thermal, and chemical stabilities of ion gels were measured under oxidative conditions as shown in **Figure 2**. The short-term stability was evaluated using a thermogravimetric analyzer, measuring transiently the change in mass of the ion gel samples as a function of temperature under flowing air (100 mL/min) and a linear temperature ramp (3 °C/min). The long-term stability of the ion gels was evaluated via two methods: (i) isothermal thermogravimetric experiments, measuring the change in mass of the ion gel at specific temperatures as a function of time, and (ii) via infrared spectroscopy (IR) experiments, tracking the chemical structure/chemical bonds of the ion gel sample isothermally as a function of time. For the transient thermogravimetric study, as shown in **Figure 2a**, the mass of the ion gel PVDF/ $[EMIM]^+[TFSI]^-$ remained constant up to 300 °C before it decomposed completely at 450 °C. For the ionic liquid $[EMIM]^+[TFSI]^-$ alone, the mass remained constant up to 225 °C before breaking down completely at 425 °C; for the polymer PVDF, the mass change remained unchanged up to 350 °C before breaking down completely at 500 °C. These results confirmed that the most stable component, polymer PVDF, imparted structural integrity to the ion gel at elevated temperatures.

Transient TGA measurements have been used extensively to evaluate the thermal stability of ion gels in prior studies; the thermogravimetric profiles of different measured ion gels typically vary depending on compositions, cationic components, anionic components, and preparation methods.[27] This is evident, as shown in Figure S5, where the shape of the TGA profile varies for the three different ion gels and their corresponding ionic liquids, keeping the same cationic component in all the ionic samples and varying only the anionic components. Therefore, to systematically quantify these transient measurements, we defined $T_{90\%}$, the temperature at which the measured mass reached 90% of its original amount and observed that the ion gel with the ionic liquid of $[EMIM]^+[TFSI]^-$ was the most stable ion gel with $T_{90\%}$ of 357 °C followed by that with $[EMIM]^+[HSO_4]^-$ at $T_{90\%}$ of 310 °C and $[EMIM]^+[CH_3COO]^-$ at $T_{90\%}$ of 198 °C as shown in **Figure 2b** and Figure S5. This parameter of $T_{90\%}$, typically used in transient TGA studies may be useful for high-throughput screening of different ion gels and ionic liquids, but it does not describe the materials' long-term stability to withstand temperatures over durations needed for catalytic applications.

The long-term stability of the ion gel made from PVDF and $[EMIM]^+[TFSI]^-$ was evaluated as shown in **Figure 2c** in isothermal thermogravimetric studies for 48 h in flowing air (100 mL/min) at temperatures of 200 °C to 300 °C in 25 °C increments. From **Figure 2c**, the mass of the ion gel remained unchanged at 200 °C after 48 h under an oxidative environment. In contrast, at 300 °C, this ion gel decomposed completely after 48 h. Isothermal oxidation at temperatures 225, 250 and 275 °C decreased the mass of the ion gel to 98%, 89%, and 68%, respectively, after 48 h. By fitting the decrease in mass over time to first order degradation kinetics, the activation energy of the ion gel degradation based on these isothermal gravimetric measurements, as shown in Figure S6-S7, was approximately 175 kJ mol^{-1}, similar to previously reported values.[28] The thermal

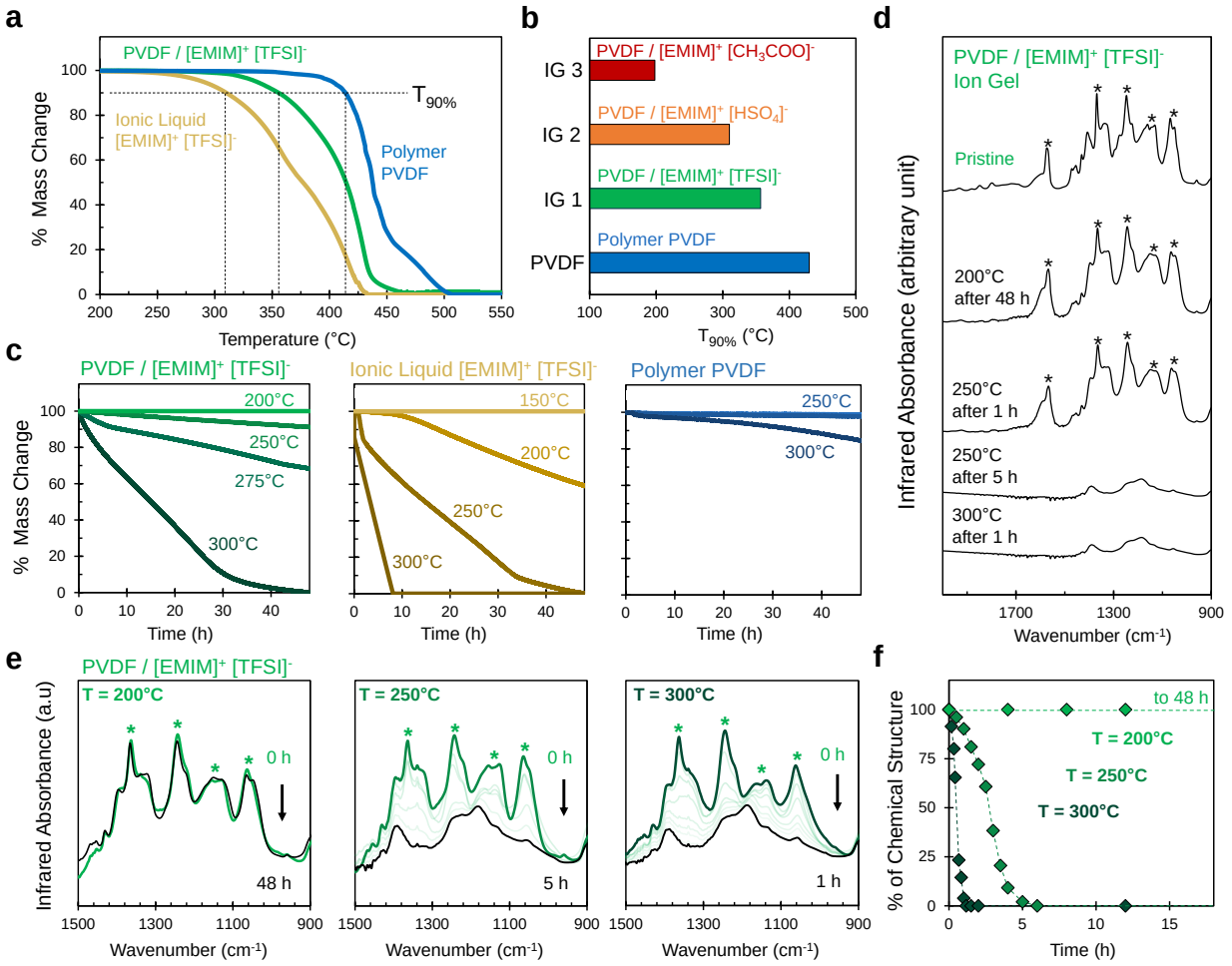

Figure 2. (a) Transient thermogravimetric analysis of polymer PVDF, ionic liquid $[EMIM]^+[TFSI]^-$, and ion gel PVDF / $[EMIM]^+[TFSI]^-$ under flowing air. $T_{90\%}$ is defined as the temperature that the change in mass reached 90%. **(b)** Comparison of the $T_{90\%}$ obtained from TGA for PVDF and three ion gels with differing anions. The stability based on anions are in the order: $[TFSI]^- > [HSO_4]^- > [CH_3COO]^-$. The TGA profile for the $[HSO_4]^-$ and $[CH_3COO]^-$ ion gels can be found in the SI. **(c)** Isothermal thermogravimetric analysis of the ion gel PVDF / $[EMIM]^+[TFSI]^-$, ionic liquid $[EMIM]^+[TFSI]^-$, and polymer PVDF over 48 h under flowing air. The ion gel maintained its mass at 100% after 48 h at 200 °C, and the ionic liquid is the least thermally stable material among the three. **(d)** IR spectra of the PVDF/ $[EMIM]^+[TFSI]^-$ ion gel held isothermally over a time. The symbol ∗ denotes the bond stretches associated with the ion gel. The ion gel maintained its chemical structure at 200 °C after 48 h. **(e)** Time-lapsed isothermal IR studies of PVDF/ $[EMIM]^+[TFSI]^-$ over time under flowing air for chemical stability assessment at 200 °C, 250 °C, and 300 °C. The symbol ∗ denotes the bond stretches associated with the ion gel. The ion gel's structure was maintained for 48 h at 200 °C. Despite better isothermal TGA profiles, the ion gel's structure degraded completely at 250 °C under both flowing air and N_2. N_2 environment did not preserve the chemical structure (See SI). **(f)** Chemical stability of the ion gel measured isothermally over time. Each point represents the integrated area within the ion gel fingerprint wavenumbers.

stabilities of the ionic liquid $[EMIM]^+[TFSI]^-$ and the polymer PVDF were also assessed isothermally for 48 h. From **Figure 2c**, the mass of the ionic liquid and the polymer PVDF remained unchanged at 100% at 150 °C and 250 °C, respectively, after 48 h. Heating the ionic liquid in flowing air at 250 °C and 300 °C completely decomposed the material after 48 h; whereas, the polymer PVDF lost only 16% of its original mass at 300 °C. Again, this result provides evidence that the polymer PVDF imparts structural support to the ionic liquid with the ionic liquid currently limiting the ion gel's overall thermal stability. Moreover, it indicates that

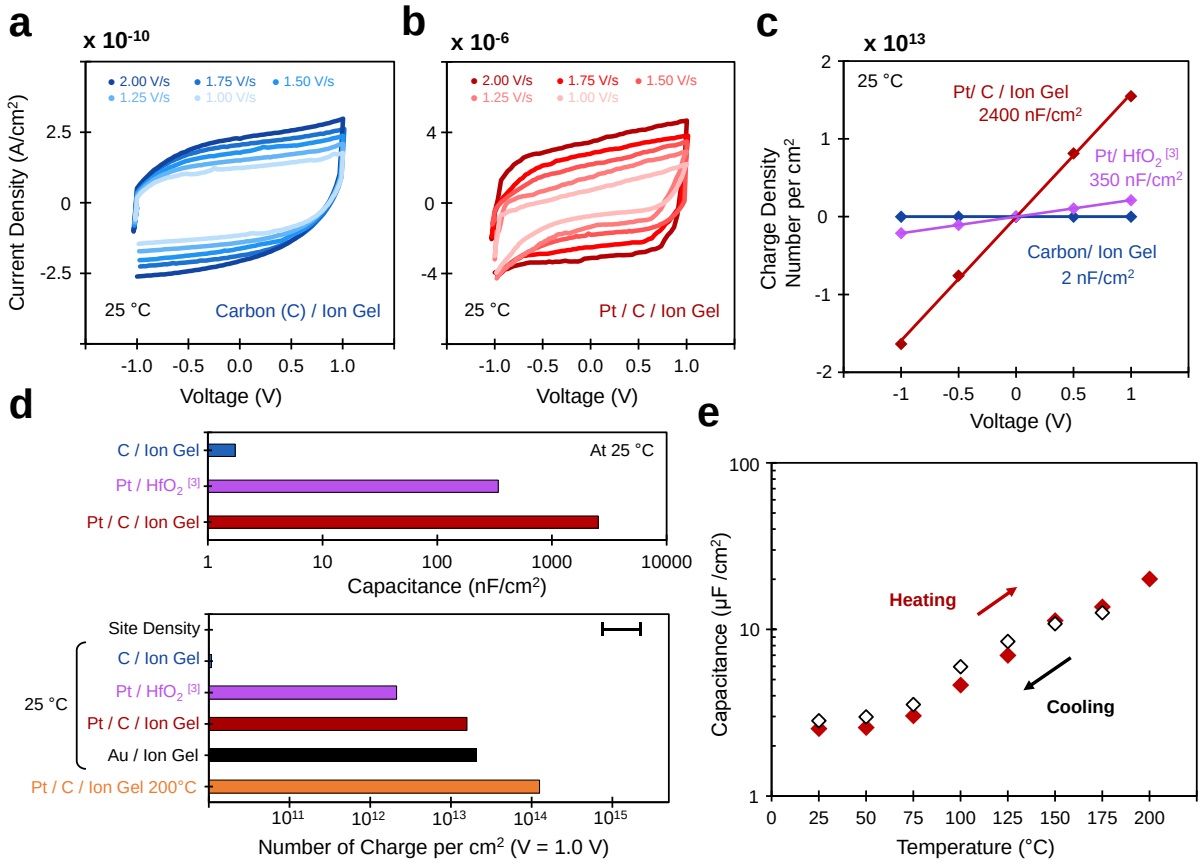

Figure 3. Electronic properties of the Pt/ C catalytic condenser with the ion gel PVDF/ $[EMIM]^+[TFSI]^-$. **(a)** *I–V* curves of C on the Ion Gel on Au-coated Si (blue) and **(b)** Pt/ C on the Ion Gel on Au-coated Si (red) at 25 °C. **(c)** Charge density measured by *I–V* curves of both devices and a reference Pt/ HfO_2/ Si from previous work as a function of applied bias V_{CAT} at 25 °C. **(d)** Device capacitance with Pt/ C/ Ion Gel (red), Pt/ HfO_2/ Si (purple), and C/ Ion Gel only (blue). Charge accumulation at ± 1 V relative to the estimated Pt active site density range. **(e)** Measured device capacitance as a function of temperature with heating and cooling.

transient TGA studies will overpredict the thermal stability of ion gels and ionic liquids.

The chemical structure of the ion gel and its thermal stability were also evaluated via infrared spectroscopy in **Figure 2d-2e**. The ion gel was first spin coated on a Au-coated Si substrate, baked, and then placed in an IR refractor reactor cell (grazing incidence) with the background of the Au-coated Si substrate subtracted. The ion gel samples were then heated to the setpoint temperatures under flowing air or flowing N_2 at 100 mL/min, matching the conditions of the thermogravimetric analyzer. IR spectra of a pristine ion gel PVDF/ $[EMIM]^+[TFSI]^-$ and its related functional groups were then compared against IR spectra of the ion gel heated at different temperatures over time. The ion gel heated at 200 °C for 48 h and the pristine sample have similar IR spectra. At 250 °C, the same bond resonances were present after 1 h of heating, but they degraded completely over 5 h under flowing air. Comparing this result to the TGA, the mass change of the ion gel after 5 h had dropped to 98%. This small difference of 2% indicates that the change in mass is not as sensitive a descriptor for the ion gel's thermal stability as IR spectroscopy. At 300 °C, the functional groups of the ion gel completely disappeared after 1 h (**Figure 2d**).

A time-resolved IR measurement of the fingerprint region between 900 and 1500 cm^{-1} under isothermal conditions was performed to characterize the stability of the ion gel's chemical structure under flowing air and flowing N_2 (**Figure 2e**). At 200 °C, the ion gel's spectra did not change after 48 h in both flowing air and flowing N_2, in agreement with the isothermal thermogravimetric measurements (results for the IR profile under

flowing N_2 are shown in Figure S9). When maintained at 250 °C, however, the IR spectra showed an eventual degradation of the chemical structure under both flowing air and flowing N_2 over 5 h and 8 h, respectively; at 300 °C, the chemical structure of the ion gel broke down completely in 1 h under both air and N_2 conditions. These observations suggest that thermal decomposition may be the primary deactivation mechanism since the exposure to N_2 environment was unable to preserve the chemical integrity of the ion gel. To evaluate the degradation kinetics of the gel's chemical stability, the integrated area of each time-lapsed spectrum was plotted over time. This chemical stability descriptor exhibited first order degradation kinetics with an R^2 greater than 0.98, and the activation energy was calculated to be 82 $\pm$ 5 kJ mol^{-1}, a value lower than that from the isothermal thermogravimetric measurement above. This suggests that the ion gel structure breaks down at lower temperatures, since the energy barrier calculated from the isothermal IR measurement is lower than that calculated from the isothermal thermogravimetric measurement. Another evidence of ion gel decomposition at lower temperatures than that suggested in the TGA measurement is a photograph of a device with a deformed surface after extensive heating at 250 °C as shown in Figure S11. This highlights the benefit of infrared spectroscopy to characterize long term stability of the ion gel structure while acknowledging that thermogravimetric measurements could be used for rapid screening of different ionic liquids and ion gels.

Ion Gel Condenser Electronic Properties at Room Temperature. The electronic properties of the Pt/ C/ Ion Gel catalytic condenser were measured as shown in **Figure 3**. To determine the amount of charge stored in the Pt layer, current-voltage (I-V) measurements were performed on both a C/Ion gel catalytic condenser (without Pt) and the full Pt/ C/ Ion gel condenser from -1.0 V to +1.0 V at different voltage sweep rates. The measured displacement current densities of the carbon ion gel condenser without Pt, as shown in **Figure 3a**, were in the range of 0.1 to 0.3 nA/cm^2, increasing linearly with sweep rate, with a calculated average specific capacitance of 1.7 nF/cm^2. The addition of Pt to the carbon ion gel condenser resulted in a significant increase in current densities, achieving ~4000 nA/cm^2, more than a thousand-fold increase over the carbon ion gel device, and a specific capacitance of 2400 nF/cm^2 when measured at room temperature (**Figure 3b**). The Pt nanoparticles added to the carbon layer increased the total capacitance of the condenser, which is consistent with charge condensing in the Pt cluster. This measurement was also conducted over the range of -3.0 V and +3.0 V, and though standard capacitance determination yielded similar values, it produced consistently a duck-shaped curve as shown in Figure S12. It is unclear whether this is caused by ions undergoing redox reaction at the interface or in the bulk, but it mimics the cyclic voltammetry curve of a typical electrochemical process.[11,29]

The accumulation of charge in the C/ Ion Gel condenser and the Pt/ C/ Ion Gel condenser are indicated by the box-shaped displacement current-voltage measurements as shown in **Figure 3a-3b**. Charge condensed on the C/ Ion Gel condenser (without Pt) was determined to be only ~10^9 (e^- or h^+) cm^{-2} for V_{CAT} of $\pm$ 1.0 V, consistent with our previous studies of carbon deposited on a different dielectric, HfO_2.[4,3] As shown in **Figures 3c-3d**, for the same potential applied on a Pt/ C/ Ion Gel condenser, the charge area density increased to ~10^{13} (e^- or h^+) cm^{-2}, with holes or electrons stabilized at V_{CAT} greater or less than zero, respectively. This order of magnitude increase suggests that charge is primarily stored in the Pt layer. The Pt addition also allows the maximum amount of charge accumulation at the applied potential for the respective ion gel; this was verified by an alternative device with a thick Au contact layer, deposited by thermal evaporation on the ion gel, in place of Pt/ C, which also stabilized ~10^{13} charges cm^{-2} at room temperature as shown in **Figure 3d**.[22]

The accumulation of charge in Pt nanoclusters can modulate the binding energy of adsorbates such as carbon monoxide (CO) and alcohols on metals and metal oxides that have catalyst site densities of ~10^{15} sites cm^{-2}. We previously reported that the charge condensed in a Pt layer on a 70 nm HfO_2 dielectric condenser was approximately ~10^{13} (e^- or h^+) cm^{-2} at V_{CAT} = $\pm$6.0 V, which corresponds to ~0.01 e^- or h^+ per active site, assuming all charge accumulates at the surface. That charge density perturbed CO binding energy by up to 0.2 eV or 20 kJ mol^{-1}. The capacitance of the ion gel reported

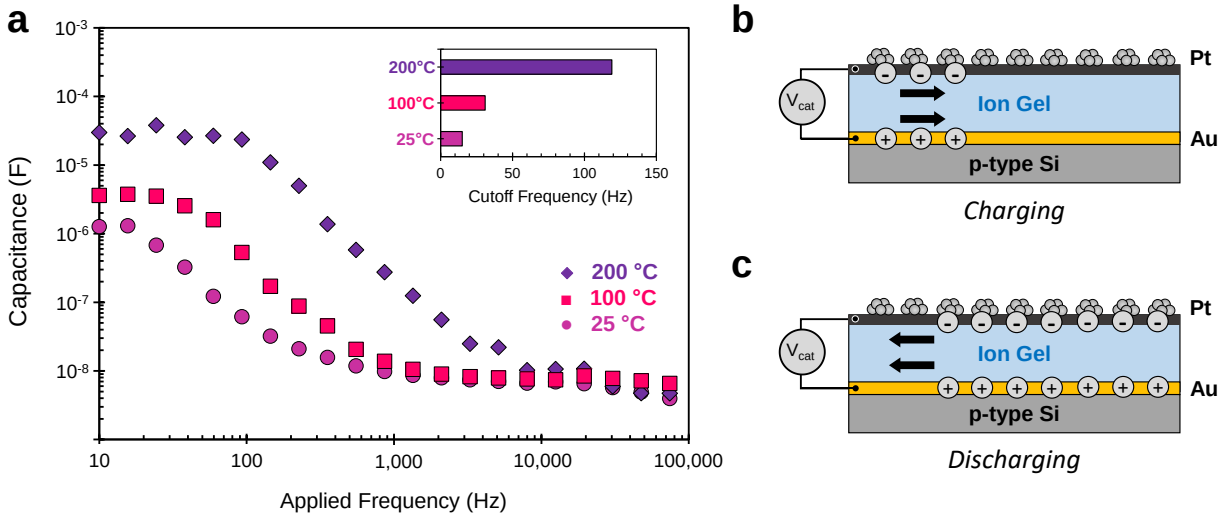

Figure 4. Dynamic electronic properties of the Pt/ C catalytic condenser with the ion gel PVDF/ $[EMIM]^+[TFSI]^-$. **(a)** Averaged capacitance of condenser devices as a function of applied frequency at 25 °C, 100 °C, and 200 °C, measured by an impedance analyzer with an inset showing cutoff frequency of each measurement**. (b)-(c)** Scheme depicting the charging and discharging mechanism of the ion gel catalytic condenser during a cyclic voltage sweep.

here being almost 10-fold that of HfO_2 suggests that it should be able to condense the same number of holes or electrons ~10^{13} cm^{-2} at a lower operating voltage of $V_{CAT} = \pm 1.0$ V; this is indeed what we find.

Temperature and Ion Gel Condenser Electronic Properties. The effects of temperature on the electronic properties of the ion gel condenser devices were assessed as shown in **Figure 3e** and **Figure 4a**. The specific capacitance of the Pt/ C/ Ion gel condenser remained constant at ~2400 nF/cm^2 from room temperature up to 50 °C, after which it increased gradually to ~20,000 nF/cm^2 when heated to 200 °C with the total amount of charge stabilized increasing by about an order of magnitude. With this capacitance, under a potential bias of 1V, an ion gel will be able to provide more than 10% charge per active site. Such an increase in capacitance with temperature is consistent with previous observations on ion gels.[30,31,32] When cooled, the capacitance of the ion gel decreased reversibly with temperature gel within experimental error. Heating to temperatures above 200 °C to 250 °C yielded inconsistent measurements of capacitances owing to the breakdown of the chemical structure of the ion gel. The I-V displacement measurements at different temperatures are shown in Figure S14.

Leakage currents, defined as the flow of electrons flowing through the ion gel layer, were also evaluated to assess the possibility of resistive heating effects on the condenser devices. To determine the leakage current, the ion gel was modeled as an equivalent circuit (See the Supporting Information). In Figure S18, the extracted leakage current also increased with operating temperature, although at 200 °C and 1.0 V potential bias, it was below conditions that would lead to any significant temperature increase (ca. 0.3 °C increase min^{-1} at 100 μA). Surface heating by leakage current was also determined to be negligible by an FLIR camera measuring the surface of the condenser device under potential application, as shown in Figure S19.

We have previously outlined strategies to achieve catalytic turnover frequencies beyond the Sabatier limit by oscillating the electronic properties of catalyst sites comparable to the natural frequencies of surface chemistry. Natural frequencies are defined as the inverse of the time constant of the rate limiting reaction step, which is typically in the range of 10 to 1,000 Hz based on models and real catalytic reactions[1,33,34]. Therefore, a criterion to achieve dynamic oscillatory rate enhancement is that the catalyst must be able to sufficiently switch between the energetic states upon perturbation. The dynamic electronic properties of the ion gel catalytic condenser were experimentally measured using an impedance spectrometer, as shown in **Figure 4a**.

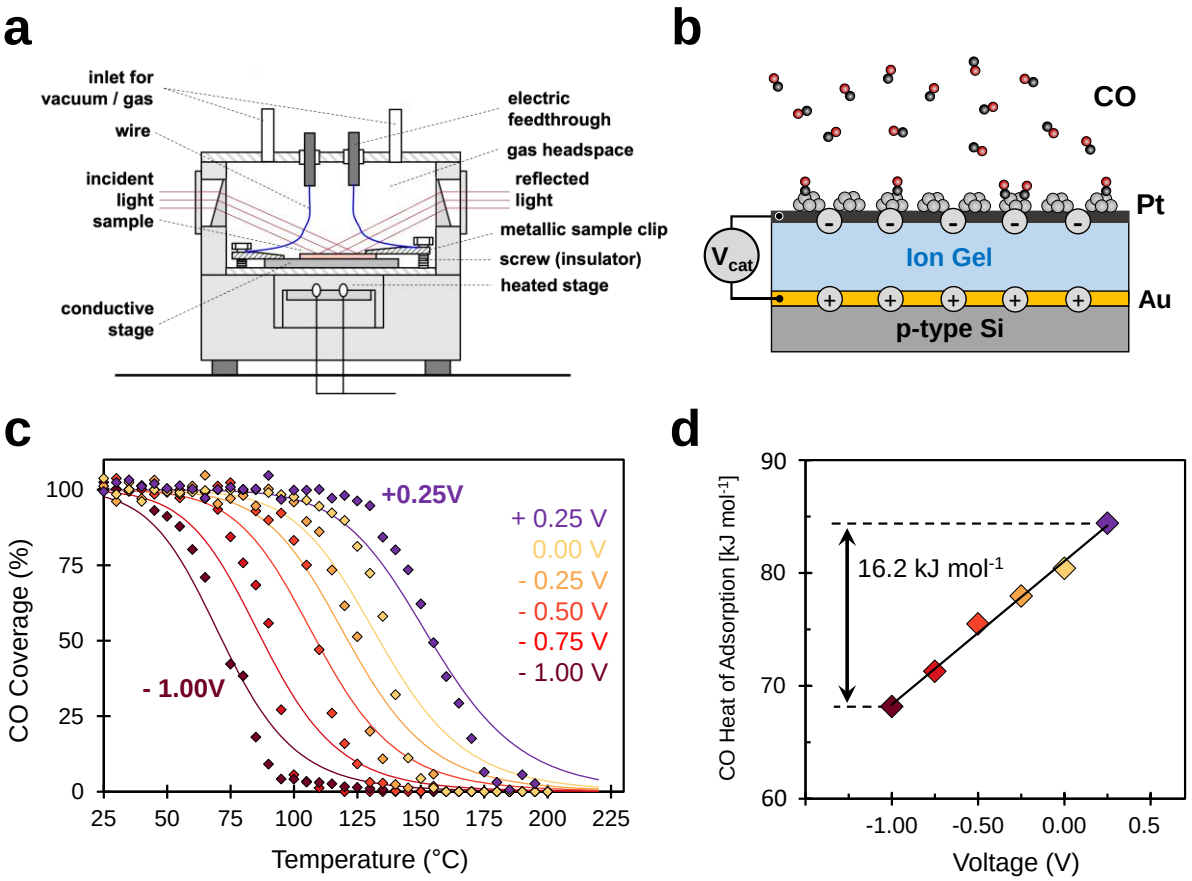

Figure 5. Infrared spectroscopy of CO on Pt/ C ion gel condenser. **(a)** Grazing incidence cell with reflected beam, heating stage, potential bias application, and gas introduction. **(b)** A schematic depicting how CO binds to the Pt surface with a characteristic broad absorbance peak at ~2080 cm^{-1} of CO after background subtraction at room temperature. The inset shows how the CO absorbance peak changes with increasing temperatures. **(c)** Adsorption isobars of the normalized CO coverage on the Pt/ C ion gel condenser measured as a function of temperature from -1.00 V to +0.25 V at 0.25 V increments. 200 °C was established as the maximum temperature before the ion gel begins to decompose. Points are experimental measurements, and lines are fitted Langmuir isobars. **(d)** Binding energy of CO on the Pt ion gel condenser determined by fitting Langmuir isobars as a function of potential biases.

The ion gel condenser at room temperature exhibited the expected ~2000 nF/cm^2 capacitance at low frequencies up to 15 Hz (cutoff frequency) and decreased to 10 nF/cm^2 as the frequency increased to 10,000 Hz. At 100 °C, the initial capacitance increased to ~4000 nF/cm^2 with the cutoff frequency also increasing to 30 Hz before the capacitance decreased again to 10 nF/cm^2 at high frequencies. At 200 °C, a capacitance of ~27,000 nF/cm^2 was measured, a tenfold increase over that at room temperature, with the cutoff frequency increasing to 120 Hz. These cutoff frequencies of 15 to 120 Hz between 25 °C and 200 °C were within the target frequencies (10 to 1,000 Hz) needed to break the Sabatier limit with opportunities for improvement.

The increase in the cutoff frequencies with temperature can be attributed to the increase in concentration of free ions within the ion gel and in ionic mobility. At elevated temperatures, interionic interactions such as hydrogen bonds deteriorate, which frees the number of ions for conduction and increases kinetic energy of mobile ions in the gel. Future work will explore more thermally stable inorganic ions such as Li^+ and thinner ion gel layers. Another opportunity to improve the cutoff frequency is to improve the lateral charge transfer across the Pt/ C sheet on the surface. While the lateral conductance of the Pt/ C is sufficient (4.7 x 10^{-3} S) for the current 1 cm^2 device, extending the device to larger areas > 5 cm^2 on different substrates may require the inclusion of metal patterns on the

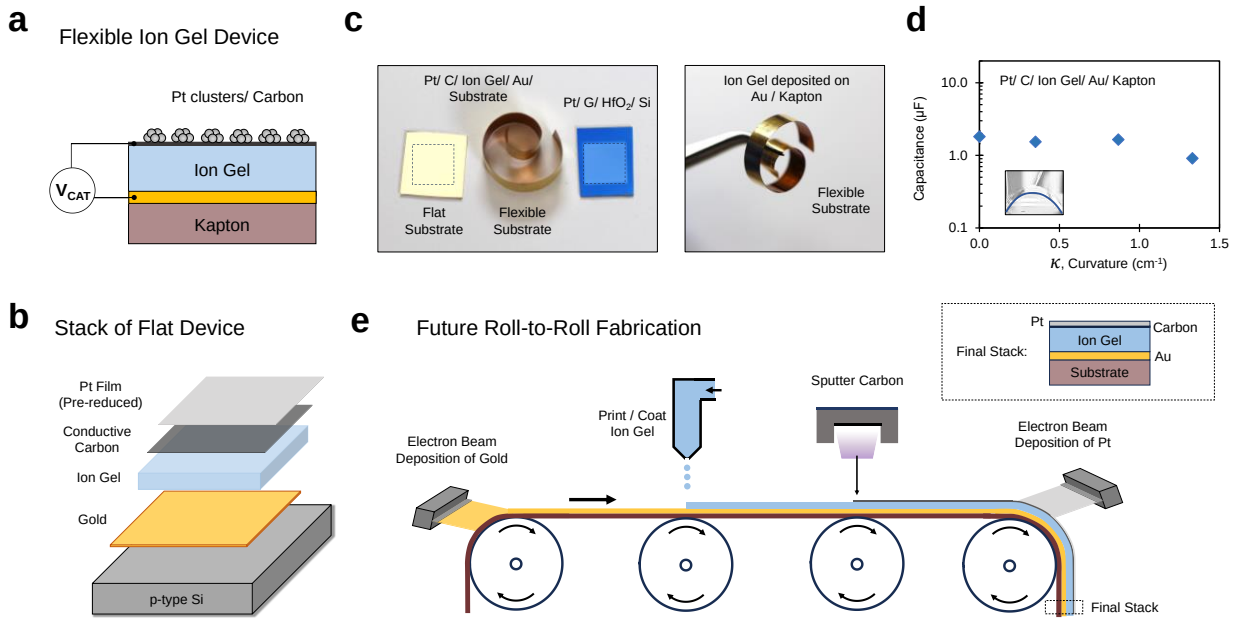

Figure 6. Flexible Ion Gel and Roll-to-Roll Printing for scalable, low-cost manufacturing. **(a)** Film stack of a Pt/ C ion gel catalytic condenser on a flexible Kapton substrate. **(b)** Illustration of the film stack of a Pt/ C ion gel catalytic condenser on a flat Si substrate. **(c)** Photographs of the ion gel condenser on a flat substrate and a flexible substrate for comparison. The square box marks a 1 cm^2 area where the Pt/ C or Pt/ Graphene was deposited. **(d)** Capacitance as a function of curvature measured for the Pt/ C on a flexible substrate undergoing tensile strain i.e., the Pt/ C/ Ion Gel stack is located at the top of curved interface. **(e)** An illustration of a promising roll-to-roll fabrication of the Pt/ C/ Ion Gel catalytic condenser with various printing technologies as options to recreate the same film stack used in this work.

carbon layer as demonstrated in our previous work.[4]

Infrared Spectroscopy and Isobars for CO Adsorption. With the Pt/ C ion gel condenser, the effects of charge on the binding energy of carbon monoxide adsorbate were experimentally determined from adsorption isobars measured via variable temperature infrared spectroscopy (VTIR).[4] The catalyst device was placed within a grazing incidence infrared spectroscopy cell (Harrick, Refractor Reactor) with the active surface of Pt/ C exposed to the incident infrared light source (**Figure 5a-5b**). A HgCdTe detector detected absorption peaks associated with surface species on the Pt/ C, subtracting the Pt/ C spectrum as the background under vacuum condition. Electrical feedthroughs supplied a fixed potential bias, V_{CAT}, to the surface of the condenser at each temperature for every isobar measurement with the bottom electrode of the condenser grounded with the entire setup. During each measurement, a fixed amount of pure CO gas (7.6 Torr) was maintained in the sample cell and over the condenser surface to maintain equilibrium between gaseous CO and surface-adsorbed species. This resulted in an adsorption spectrum with a broad peak for CO* on Pt at 2080 cm^{-1} under fixed CO(g) partial pressure, distinct from the two gaseous CO vibrational modes peaks at 2143 and 2269 cm^{-1}.[35,36,37]

To measure the CO adsorption isobars, the sample temperature (measured with a thermocouple within the sample cell) was allowed to equilibrate for one minute for each experimental data point to allow sufficient exposure of gaseous CO and the Pt surface. CO adsorption isobars were acquired for potential biases, V_{CAT}, from -1.00 to +0.25 V at 0.25 V increments between 25 to 200 °C, the thermal stability limit of the ion gel (**Figure 5c**). The isobars were normalized to the isobar area measurements obtained at 25 °C accounting also for drifts in the baseline at each temperature (i.e., IR spectrum of the sample only was obtained at every temperature increment to account for the thermal drift in baseline); the peak area decreased with increasing temperature consistent with reduced surface coverage of an exothermic CO adsorption on Pt. An in-situ displacement current measurement at a voltage sweep rate was obtained from the

condenser device prior to each run. From the isobar data shown in **Figure 5c**, negative biases (-1.00 V to -0.25 V) weakened the CO* binding energy, shifting the adsorption isobar to lower temperatures, while positive potential bias (+0.25V) strengthened the binding of CO* on the Pt surface, moving the isobars to higher temperatures. Higher positive voltages were not considered in this particular experiment, as the isobars could exceed the thermal stability limit established for the ion gel at 200 °C.

The change in the CO binding energy with applied potential bias was evaluated from the isobars using Langmuir isobar models (see Supporting Information for details). With the assumption that the adsorbed CO is immobilized on the Pt surface (ΔS_{ads} of 197 J mol^{-1} K^{-1}),[38] the heat of adsorption of CO was determined for the potential bias from -1.00 V to +0.25 V (**Figure 6d**). The ion gel condensers with a capacitance of 2400 nF/ cm^2 modulated the CO binding energy from 68.2 to 84.4 kJ mol^{-1} over a range of 16.2 kJ mol^{-1}, and the trend of the increasing CO binding energy with decreasing electron density in the Pt/ C layer on the ion gel was consistent with our previous observation on Pt/ Graphene/HfO_2 condensers with a capacitance of 340 nF/ cm^2 though at higher potential biases of $\pm$ 6.00 V. This result highlights the considerable charge storage capacity of the ion gel that enables future opportunities to tune the energy profile of a catalytic cycle to enhance surface chemistry efficiently at low applied voltages.

Flexible and Extended Ion Gels for Roll-to-roll Fabrication. Fabrication of ion gel devices with high capacitance for portable and wearable electronics using printing processes and roll-to-roll techniques has been reported over the last decade.[39,40,41,42] This is possible in part due to the gel's enabling features of excellent mechanical durability, flexibility, and large area scalability. Flexible substrates offer routes to higher-aspect-ratio structures when folded and coiled, which exhibit higher surface areas for applications in catalysis and separations in which the active surface must interact with a fluid phase. Increasing the total number of active sites using a flexible substrate is essential for future catalyst dynamics applications in important industrial chemistries such as ammonia synthesis, CO_2 hydrogenation, and water-splitting. As shown in the cartoon on **Figure 6a-6b**, a flexible ion gel condenser was fabricated on a Kapton substrate which supported the Pt/ C/ Ion Gel/ Au film stack, prepared via the same procedure as that on the p-type Si substrate. Other metals such as Fe or Al could readily replace Au as a back electrode for manufacturing feasibility, but for the purpose of comparison this film stack used Au. The photographs on **Figure 6c** further highlight the difference in form factors of the flexible Pt/ C condenser and that of the Pt condensers for this current work and our previous work; the flexible substrate combined with films of metal, carbon, and ion gel can bend and curl.

The electronic properties of the Pt/ C/ ion gel flexible condenser were evaluated for varying extent of curvature in **Figure 6d** with the respective I-V curves shown in the Supporting Information. To create curvature with the film stack, one side of the condenser was first held fixed by tape to a surface. Pressure was then applied on the other side of the flexible condenser to create curvature with the movable side of the condenser later held fixed by a weight. Tungsten probe tips were then placed gently on the Pt/ C layer and the Au electrode layer. The capacitance of a 1 cm^2 flexible ion gel condenser remained constant at ~ 2000 nF/ cm^2 for curvatures less than 1 cm^{-1} (κ < 1 cm^{-1}) and decreased to 930 nF/ cm^2 for high curvatures of κ = 1.3 cm^{-1}. A flexible metal substrate is also desirable for thermal catalytic applications, where elevated temperatures above 400 °C degrade substrates such as Kapton over time.

Ion gels provide versatility in ionic liquid composition selection, adaptability and self-healing, mechanical stability, and excellent electronic properties which surpass high-*k* metal oxides such as HfO_2 for condensing charge in active layers to electronically modulate adsorbates on metals and metal oxides. For ion gels to be applicable in heterogeneous catalysts, the total number of active sites and active site density within the entire ion gel device must be increased. Fabrication of the catalytic condenser film stack on flexible substrates using high-throughput, roll-to-roll techniques are manufacturing processes that can create foldable catalysts with higher aspect ratios and consequently higher active site density. **Figure 6e** shows a proposed roll-to-roll process integrated with established deposition techniques such as e-beam metal deposition,[43,44] printing,[45]

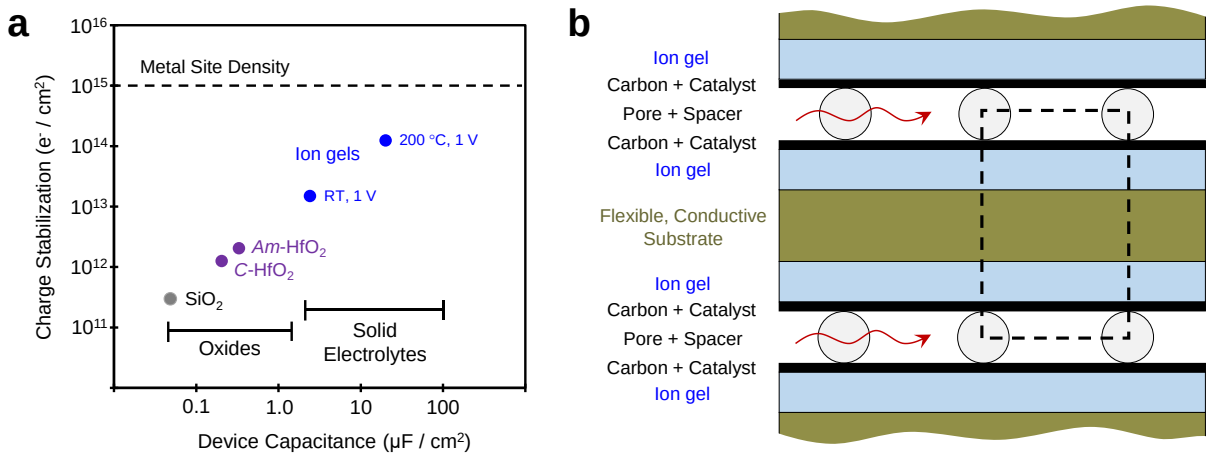

Figure 7. Implications of ion gel catalytic condensers. **(a)** The capacitance of the catalytic condensers increases with different insulating dielectric layers of silica, amorphous and crystalline HfO_2, and ion gel at room temperature and 200 °C for applied voltage of 1 V. **(b)** Combination of multiple catalytic condenser films can be combined with insulating spacers to permit high active site density and pores for flow of reactant gases.

coating,[46] and carbon sputtering[47,48] to continuously manufacture the catalytic condenser film stacks. Among these techniques, printing offers a low-cost, scalable process that avoids vacuum operations. Different printing methods, such as gravure, inkjet, and aerosol jet, have already demonstrated the printability of different metals, metal oxides, graphene, and other organic species in recent works.[49,50,51,52,53] The scaling up of ion gels for dynamic and programmable modulation of catalysts may offer opportunities to drive industrially important chemistries more efficiently.

Implications of Ion Gels for Catalytic Condensers. The ability to coat or print ion gels on flexible substrates enables significantly more powerful and scalable catalytic condenser devices (**Figure 7**). The common dielectric of silica with film thicknesses of ~100 nm exhibits capacitances below 0.1 μF/cm^2; capacitance increases significantly when switching to either crystalline (C) or amorphous (Am) ~100 nm HfO_2 films (**Figure 7a**). Yet, HfO_2 dielectric films condense at most 5 x 10^{13} e$^-$/cm^2, which is 20X fewer electrons than the approximate areal density of active sites on metal surface (~10^{15} sites/cm^2). At room temperature ion gel films 3.8 μm thick exhibit capacitance above 1.0 μF/cm^2, and for voltages above 1 V, they can condense ~10^{13} e$^-$/cm^2. At higher temperatures of 200 °C relevant for catalysis applications, ion gel films can stabilize ~10^{14} e$^-$/cm^2, which means nearly 0.1 electron or hole per metal active site. This extent of charge condensation is approximately an order of magnitude higher than earlier HfO_2 devices, allowing for significant adsorbate binding energy variation on catalytic surfaces. As shown previously via simulation, increases in binding energy amplitude in surface oscillation provide logarithmic increases in catalytic turnover frequency, making it one of the key characteristics of dynamic active sites.[2,54]

The ability to mass produce condensers made of ion gels on continuous and flexible sheets also increases the ability to produce high active site density devices. As depicted in **Figure 7b**, the catalytic condenser architecture can be stacked as either single- or double-sided layers with insulating spaces between the films; for example, silica beads would pillar the layers while allowing for the flow of reactant gases (red arrows) to access active sites. This architecture could be implemented as stacked flat sheets or a rolled-up cylinder 'jelly-roll' device with electrical contacts extending axially out of the device. The catalyst active site density can be approximated geometrically (see the dashed line box of **Figure 7b**). For a flat double-sided condenser sheet stack with silica bead spacers of 5 μm diameter, a conductive substrate of 15 μm, an ion gel thickness of 3.8 μm, with a metal areal density of 10^{15} sites/cm^2, the active site density is

approximately 4 x 10^{17} sites/cm^3. Further folding or rolling the substrates may increase the volumetric site density by an order of magnitude or more in the goal of attaining site densities viable for industrial applications. Introductions of grooved surfaces to the conductive substrate to build the condenser stack can also increase the site density. Combined with scalable and low-cost manufacturing process such as roll-to-roll printing, the methodology of dynamically perturbing catalytic sites with charge becomes an intriguing option in catalysis.

3.0 Experimental Methods. Experimental Methods. The platinum carbon ion gel catalytic condenser was fabricated, and its structure, thermal stability, electronic property, and catalytic property were determined using microscopy, profilometry, infrared spectroscopy, displacement current measurement, and impedance spectroscopy. Complete research methods are described in the Supporting Information.

Ion Gel Catalytic Condenser Fabrication. The catalytic condensers were fabricated on a conductive p-type Si substrate (WaferPro) with sequential deposition of Au/Ti, ion gel, conductive carbon, and Pt layer. First, a 45 nm Au and 5 nm Ti contact layer were deposited on the Si substrate by e-beam deposition of pure Au and Ti sources, respectively. Any mention of Au layer in the text refers to a layer of 45 nm Au with a 5 nm Ti adhesion layer. Subsequently, a solution of the ion gel (7.7 wt. % polyvinylidene difluoride or PVDF polymer, 30.8 wt. % 1-ethyl-3-methylimidazolium bis(trifluoromethylsulfonyl) imide or $[EMIM]^+[TFSI]^-$ ionic liquid, 61.5 wt. % acetone solvent) was prepared by stirring all components in a vial submerged in a silicone oil bath at 60 °C until full polymer dissolution. The ion gel solution was spin coated (4500 rpm, 60 s) on the Au-coated substrate in a clean room. The deposited gel on the substrate was then dried in a vacuum oven for 24 h at 70 °C to remove the acetone. With a shadow mask as a template, a 1.0 cm^2 area of conductive carbon (1.8 nm thick) was sputtered on top of the ion gel using a sputter coater (Leica EM ACE600) by pulsing carbon thread at 140 W under high vacuum (~10^{-5} torr). A Pt layer (target of 1 nm) was then grown on the conductive carbon by e-beam evaporation of a pure Pt source. Two other ionic liquids were also explored in the thermal studies. For the flexible substrate, the same procedure of spin coating ion gel, carbon sputtering, and e-beam deposition of Pt was repeated on a Kapton substrate (American Durafilm). Full descriptions of the fabrication process are available in the Supporting Information.

Profilometry and Scanning Electron Microscopy. The thickness of the ion gel was measured using a profilometer (KLA-Tencor P-7) over a scan area of 500 µm at a scan speed of 10 µm/s and rate of 1000 Hz. SEM images and SEM-EDX maps were acquired using JEOL 6500 FEG-SEM. SEM images and SEM-EDX elemental maps were acquired under 5 kV. The SEM-EDX maps were quantified using the Aztec EDX analytical system (Oxford Instruments).

Spectroscopy. XPS spectra collection was performed on a PHI Versa Probe III XPS system (ULVAC-PHI) using a mono-chromated Al Kα X-ray source (1486.6 eV). The measurements were conducted using an X-ray spot size of 0.1 × 0.1 mm^2 with a power of 25 W under 15 kV. The survey spectra were measured using 280 eV pass energy and 1.0 eV/step. The data was processed with the Multipak software. Infrared spectra of the ion gel and the platinum ion gel condenser devices exposed to CO were collected using a Thermo Scientific Nicolet iS50 FT-IR with a Mercury-Cadmium-Telluride (MCT) detector and a tailored Refractor Reactor Grazing Angle setup (Harrick Scientific). The incident angle of the reactor was fixed at 75°, and the windows used were wedged ZnSe. To measure the effects of temperature with IR, the background was first collected at every experimental temperature. For the thermal stability study involving ion gel deposited on the Au coated substrate, a Au-only substrate was used as the background for subtraction. For the CO desorption study, the Pt ion gel catalytic condenser device was used as the background for subtraction. During an experimental run, pure CO (~7.6 Torr) was dosed into the sample chamber and the IR spectrum was then collected and subtracted. Full details on collections and analyses are available in the Supporting Information.

Device Electronic Characterization. Capacitance measurements were collected from a probe station equipped with a source meter (Keithley 2611B and Keithley Test Script Builder). Conductive metal probes were carefully placed on the surface of the sample for the electrical measurements. Different voltage sweep-rates (2.00

V/s, 1.75 V/s, 1.50 V/s, 1.25 V/s, 1.00 V/s) were used to collect the I-V curves. For temperature-based experiments, a conductive sample stage was placed on top of a ceramic non-conductive hot plate. Probes were carefully placed on the sample's surface and on the conductive stage to measure capacitance and leakage current. The impedance spectra of the devices were recorded in the same two-electrode configuration, like the setup used in capacitance measurement as described above. These measurements were performed with a Newtons PSM3750 multimeter equipped with an Impedance Analysis Interface 2 from the frequency range of 10 Hz to 10 MHz.

4.0 Conclusions. A Pt on C ion gel catalytic condenser was fabricated, characterized, and evaluated for its thermal stability and its electronic ability to modulate the binding energy of carbon monoxide with varying applied potential. The ion gel condenser film stack is configured with exposed Pt/ Carbon active sites available to an external fluid for catalytic reactions and separation applications. Starting with a Au-deposited Si substrate, ion gel was first spin coated to yield a ~3.8 μm film. Conductive carbon was then sputtered on top of the ion gel followed by the deposition of Pt by electron beam deposition. Electron microscopy and X-ray photoelectron spectroscopy confirmed the surface structure and elemental makeup of the stack, showing no agglomerate formation. The thermal stability of three PVDF/ $[EMIM]^+[Anion]^-$ ion gels with differing anion species were assessed via transient and isothermal thermogravimetric measurements and isothermal infrared spectroscopy (IR) over 48 h. The isothermal IR measurement provided the best assessment of the thermal stability of the ion gel's chemical structure, the most stable being the PVDF/ $[EMIM]^+[TFSI]^-$ ion gel. For electronic characterization, accumulation of charge in the Pt/ C layer of the ion gel condensers of capacitance 2400 nF/cm^2 amounted to ~10^{14} e^-/cm^2 under a potential bias of $\pm$ 1 V with a cutoff frequency of 15 Hz. The capacitance and the cutoff frequency of the ion gel improved to 20,000 nF/ cm^2 and 120 Hz respectively at 200 °C, providing a significant ~10% charge per active site at $\pm$ 1 V. CO binding on Pt was then evaluated by measuring adsorption isobars from temperatures of 25 to 200 °C under a fixed bias of -1.00 V to +0.25 V at 0.25 V increments. The CO binding energy, through fitting a Langmuir isobar, was estimated to shift from 68.2 to 84.4 kJ mol^{-1} over the applied potential range; larger variation in CO binding was possible with higher voltages but was not detectable by spectroscopic methods. Finally, ion gel, with its excellent mechanical properties, can be fabricated via a scalable and low-cost manufacturing process in as roll-to-roll printing, creating more active sites over a volume of space and enabling dynamic perturbation with charge to become industrially relevant in catalytic applications.

Acknowledgements. This work was supported as part of the Center for Programmable Energy Catalysis, an Energy Frontier Research Center funded by the U.S. Department of Energy, Office of Science, Basic Energy Sciences at the University of Minnesota under award #DE-SC0023464.

Keywords. Energy, Catalysis, Storage, Dynamics

Supporting Information. Additional details including the calculation of the turnover efficiency are available in the supporting information (Section S4); additional methods of data extrapolation (Section S3) and batch reactor covariance analysis (Section S7-1) are also included. Digital copies of the data tables are available at the Data Repository of the University of Minnesota (DRUM).

References

(1) Shetty, M.; Walton, A.; Gathmann, S. R.; Ardagh, M. A.; Gopeesingh, J.; Resasco, J.; Birol, T.; Zhang, Q.; Tsapatsis, M.; Vlachos, D. G.; Christopher, P.; Frisbie, C. D.; Abdelrahman, O. A.; Dauenhauer, P. J. The Catalytic Mechanics of Dynamic Surfaces: Stimulating Methods for Promoting Catalytic Resonance. *ACS Catal.* **2020**, 12666–12695. https://doi.org/10.1021/acscatal.0c03336.

(2) Ardagh, M. A.; Abdelrahman, O. A.; Dauenhauer, P. J. Principles of Dynamic Heterogeneous Catalysis: Surface Resonance and Turnover Frequency Response. *ACS Catal.* **2019**, *9* (8), 6929–6937. https://doi.org/10.1021/acscatal.9b01606.

(3) Onn, T. M.; Gathmann, S. R.; Wang, Y.;

Patel, R.; Guo, S.; Chen, H.; Soeherman, J. K.; Christopher, P.; Rojas, G.; Mkhoyan, K. A.; Neurock, M.; Abdelrahman, O. A.; Frisbie, C. D.; Dauenhauer, P. J. Alumina Graphene Catalytic Condenser for Programmable Solid Acids. *JACS Au* **2022**. https://doi.org/10.1021/jacsau.2c00114.

(4) Onn, T. M.; Gathmann, S. R.; Guo, S.; Solanki, S. P. S.; Walton, A.; Page, B. J.; Rojas, G.; Neurock, M.; Grabow, L. C.; Mkhoyan, K. A.; Abdelrahman, O. A.; Frisbie, C. D.; Dauenhauer, P. J. Platinum Graphene Catalytic Condenser for Millisecond Programmable Metal Surfaces. *J. Am. Chem. Soc.* **2022**, *144* (48), 22113–22127. https://doi.org/10.1021/jacs.2c09481.

(5) Ardagh, M. A.; Birol, T.; Zhang, Q.; Abdelrahman, O. A.; Dauenhauer, P. J. Catalytic Resonance Theory: SuperVolcanoes, Catalytic Molecular Pumps, and Oscillatory Steady State. *Catal. Sci. Technol.* **2019**, *9* (18), 5058–5076. https://doi.org/10.1039/c9cy01543d.

(6) Dauenhauer, P. J.; Ardagh, M. A.; Shetty, M.; Kuznetsov, A.; Zhang, Q.; Christopher, P.; Vlachos, D. G.; Abdelrahman, O. A. Catalytic Resonance Theory: Parallel Reaction Pathway Control. *Chem. Sci.* **2020**, *11* (13), 3501–3510. https://doi.org/10.1039/c9sc06140a.

(7) Gathmann, S. R.; Ardagh, M. A.; Dauenhauer, P. J. Catalytic Resonance Theory: Negative Dynamic Surfaces for Programmable Catalysts. *Chem Catal.* **2022**. https://doi.org/10.1016/j.checat.2021.12.006.

(8) Kim, Y. M.; Choi, W. Y.; Kwon, J. H.; Lee, J. K.; Moon, H. C. Functional Ion Gels: Versatile Electrolyte Platforms for Electrochemical Applications. *Chem. Mater.* **2021**, *33* (8), 2683–2705. https://doi.org/10.1021/acs.chemmater.1c00330.

(9) Kushida, S.; Kebrich, S.; Smarsly, E.; Strunk, K.-P.; Melzer, C.; Bunz, U. H. F. Light-Emitting Electrochemical Cells Based on Conjugated Ion Gels. *ACS Appl. Mater. Interfaces* **2020**, *12* (34), 38483–38489. https://doi.org/10.1021/acsami.0c11951.

(10) Sato, S.; McNicholas, B. J.; Grubbs, R. H. Aqueous Electrocatalytic CO2 Reduction Using Metal Complexes Dispersed in Polymer Ion Gels. *Chem. Commun.* **2020**, *56* (32), 4440–4443. https://doi.org/10.1039/D0CC00791A.

(11) Taghavikish, M.; Subianto, S.; Gu, Y.; Sun, X.; Zhao, X. S.; Choudhury, N. R. A Poly(Ionic Liquid) Gel Electrolyte for Efficient All Solid Electrochemical Double-Layer Capacitor. *Sci. Rep.* **2018**, *8* (1), 10918. https://doi.org/10.1038/s41598-018-29028-y.

(12) Narasimhan, V.; Park, S.-Y. An Ion Gel as a Low-Cost, Spin-Coatable, High-Capacitance Dielectric for Electrowetting-on-Dielectric (EWOD). *Langmuir* **2015**, *31* (30), 8512–8518. https://doi.org/10.1021/acs.langmuir.5b01745.

(13) Lee, J.; Kaake, L. G.; Cho, J. H.; Zhu, X.-Y.; Lodge, T. P.; Frisbie, C. D. Ion Gel-Gated Polymer Thin-Film Transistors: Operating Mechanism and Characterization of Gate Dielectric Capacitance, Switching Speed, and Stability. *J. Phys. Chem. C* **2009**, *113* (20), 8972–8981. https://doi.org/10.1021/jp901426e.

(14) Membreno, D.; Smith, L.; Shin, K.-S.; Chui, C. O.; Dunn, B. A High-Energy-Density Quasi-Solid-State Carbon Nanotube Electrochemical Double-Layer Capacitor with Ionogel Electrolyte. *Transl. Mater. Res.* **2015**, *2* (1), 15001. https://doi.org/10.1088/2053-1613/2/1/015001.

(15) Isik, M.; Lonjaret, T.; Sardon, H.; Marcilla, R.; Herve, T.; Malliaras, G. G.; Ismailova, E.; Mecerreyes, D. Cholinium-Based Ion Gels as Solid Electrolytes for Long-Term Cutaneous Electrophysiology. *J. Mater. Chem. C* **2015**, *3* (34), 8942–8948. https://doi.org/10.1039/C5TC01888A.

(16) Lee, K. H.; Zhang, S.; Lodge, T. P.; Frisbie, C. D. Electrical Impedance of Spin-Coatable Ion Gel Films. *J. Phys. Chem. B* **2011**, *115* (13), 3315–3321. https://doi.org/10.1021/jp110166u.

(17) Wang, D.; Zhao, S.; Yin, R.; Li, L.; Lou, Z.; Shen, G. Recent Advanced

Applications of Ion-Gel in Ionic-Gated Transistor. *npj Flex. Electron.* **2021**, *5* (1), 13. https://doi.org/10.1038/s41528-021-00110-2.

(18) Cho, K. G.; Cho, Y. K.; Kim, J. H.; Yoo, H.; Hong, K.; Lee, K. H. Thermostable Ion Gels for High-Temperature Operation of Electrolyte-Gated Transistors. *ACS Appl. Mater. Interfaces* **2020**, *12* (13), 15464–15471. https://doi.org/10.1021/acsami.9b23358.

(19) Jamil, R.; Silvester, D. S. Ionic Liquid Gel Polymer Electrolytes for Flexible Supercapacitors: Challenges and Prospects. *Curr. Opin. Electrochem.* **2022**, *35*, 101046. https://doi.org/https://doi.org/10.1016/j.coelec.2022.101046.

(20) Kim, S. Y.; Jang, Y. J.; Kim, Y. M.; Lee, J. K.; Moon, H. C. Tailoring Diffusion Dynamics in Energy Storage Ionic Conductors for High-Performance, Multi-Function, Single-Layer Electrochromic Supercapacitors. *Adv. Funct. Mater.* **2022**, *32* (25), 2200757. https://doi.org/https://doi.org/10.1002/adfm.202200757.

(21) Dechiraju, H.; Jia, M.; Luo, L.; Rolandi, M. Ion-Conducting Hydrogels and Their Applications in Bioelectronics. *Adv. Sustain. Syst.* **2022**, *6* (2), 2100173. https://doi.org/https://doi.org/10.1002/adsu.202100173.

(22) Lee, K. H.; Kang, M. S.; Zhang, S.; Gu, Y.; Lodge, T. P.; Frisbie, C. D. "Cut and Stick" Rubbery Ion Gels as High Capacitance Gate Dielectrics. *Adv. Mater.* **2012**, *24* (32), 4457–4462. https://doi.org/https://doi.org/10.1002/adma.201200950.

(23) Jung, E. M.; Lee, S. W.; Kim, S. H. Printed Ion-Gel Transistor Using Electrohydrodynamic (EHD) Jet Printing Process. *Org. Electron.* **2018**, *52*, 123–129. https://doi.org/https://doi.org/10.1016/j.orgel.2017.10.013.

(24) Song, D.; Zare Bidoky, F.; Secor, E. B.; Hersam, M. C.; Frisbie, C. D. Freestanding Ion Gels for Flexible, Printed, Multifunctional Microsupercapacitors. *ACS Appl. Mater. Interfaces* **2019**, *11* (10), 9947–9954. https://doi.org/10.1021/acsami.8b20766.

(25) Jeong, J.; Marques, G. C.; Feng, X.; Boll, D.; Singaraju, S. A.; Aghassi-Hagmann, J.; Hahn, H.; Breitung, B. Ink-Jet Printable, Self-Assembled, and Chemically Crosslinked Ion-Gel as Electrolyte for Thin Film, Printable Transistors. *Adv. Mater. Interfaces* **2019**, *6* (21), 1901074. https://doi.org/https://doi.org/10.1002/admi.201901074.

(26) Oh, K.-R.; Onn, T. M.; Walton, A.; Frisbie, D.; Dauenhauer, P. J. Fabrication of Large Metal on Carbon Catalytic Condensers for Programmable Catalysis. **2023**.

(27) Xu, C.; Cheng, Z. Thermal Stability of Ionic Liquids: Current Status and Prospects for Future Development. *Processes*. 2021. https://doi.org/10.3390/pr9020337.

(28) de Jesus Silva, A. J.; Contreras, M. M.; Nascimento, C. R.; da Costa, M. F. Kinetics of Thermal Degradation and Lifetime Study of Poly(Vinylidene Fluoride) (PVDF) Subjected to Bioethanol Fuel Accelerated Aging. *Heliyon* **2020**, *6* (7), e04573. https://doi.org/https://doi.org/10.1016/j.heliyon.2020.e04573.

(29) Dutta, A.; Mishra, D. K.; Kundu, D.; Mahanta, U.; Jiang, S. P.; Silvester, D. S.; Banerjee, T. Examining the Electrochemical Nature of an Ionogel Based on the Ionic Liquid [P66614][TFSI] and TiO2: Synthesis, Characterization, and Quantum Chemical Calculations. *Ind. Eng. Chem. Res.* **2022**, *61* (25), 8763–8774. https://doi.org/10.1021/acs.iecr.2c00550.

(30) Sivaneri, K. V. I.; Ozmen, O.; Aziziha, M.; Sabolsky, E. M.; Evans, T. H.; DeVallance, D. B.; Johnson, M. B. Robust Polymer-HfO2 Thin Film Laminar Composites for Tactile Sensing Applications. *Smart Mater. Struct.* **2019**, *28* (2), 25002. https://doi.org/10.1088/1361-665X/aae00f.

(31) Yong, H.; Park, H.; Jung, C. Quasi-Solid-State Gel Polymer Electrolyte for a Wide Temperature Range Application of Acetonitrile-Based Supercapacitors. *J. Power Sources* **2020**, *447*, 227390. https://doi.org/https://doi.org/10.1016/j.jpowsour.2019.227390.

(32) Le Fevre, L. W.; Ejigu, A.; Todd, R.; Forsyth, A. J.; Dryfe, R. A. W. High Temperature Supercapacitors Using Water-in-Salt Electrolytes: Stability above 100 °C. *Chem. Commun.* **2021**, *57* (43), 5294–5297. https://doi.org/10.1039/D1CC01087E.

(33) Gopeesingh, J.; Ardagh, M. A.; Shetty, M.; Burke, S. T.; Dauenhauer, P. J.; Abdelrahman, O. A. Resonance-Promoted Formic Acid Oxidation via Dynamic Electrocatalytic Modulation. *ACS Catal.* **2020**, *10* (17), 9932–9942. https://doi.org/10.1021/acscatal.0c02201.

(34) R., W. G.; Shizhong, L.; J., D. P.; G., V. D. Catalytic Resonance of Ammonia Synthesis by Simulated Dynamic Ruthenium Crystal Strain. *Sci. Adv.* **2022**, *8* (4), eabl6576. https://doi.org/10.1126/sciadv.abl6576.

(35) Borchert, H.; Fenske, D.; Kolny-Olesiak, J.; Parisi, J.; Al-Shamery, K.; Bäumer, M. Ligand-Capped Pt Nanocrystals as Oxide-Supported Catalysts: FTIR Spectroscopic Investigations of the Adsorption and Oxidation of CO. *Angew. Chemie - Int. Ed.* **2007**, *46* (16), 2923–2926. https://doi.org/10.1002/anie.200604460.

(36) Lan, J.; Hutter, J.; Iannuzzi, M. First-Principles Simulations of an Aqueous CO/Pt(111) Interface. *J. Phys. Chem. C* **2018**, *122* (42), 24068–24076. https://doi.org/10.1021/acs.jpcc.8b05933.

(37) Ding, K.; Gulec, A.; Johnson, A. M.; Schweitzer, N. M.; Stucky, G. D.; Marks, L. D.; Stair, P. C. Identification of Active Sites in CO Oxidation and Water-Gas Shift over Supported Pt Catalysts. *Science (80-.).* **2015**, *350* (6257), 189–192. https://doi.org/10.1126/science.aac6368.

(38) NIST Webbook https://webbook.nist.gov/ (accessed Jul 30, 2022).

(39) Ovhal, M. M.; Kumar, N.; Lee, H. B.; Tyagi, B.; Ko, K.-J.; Boud, S.; Kang, J.-W. Roll-to-Roll 3D Printing of Flexible and Transparent All-Solid-State Supercapacitors. *Cell Reports Phys. Sci.* **2021**, *2* (9), 100562. https://doi.org/https://doi.org/10.1016/j.xcrp.2021.100562.

(40) Palavesam, N.; Marin, S.; Hemmetzberger, D.; Landesberger, C.; Bock, K.; Kutter, C. Roll-to-Roll Processing of Film Substrates for Hybrid Integrated Flexible Electronics. *Flex. Print. Electron.* **2018**, *3* (1), 14002. https://doi.org/10.1088/2058-8585/aaaa04.

(41) Lee, K. H.; Zhang, S.; Gu, Y.; Lodge, T. P.; Frisbie, C. D. Transfer Printing of Thermoreversible Ion Gels for Flexible Electronics. *ACS Appl. Mater. Interfaces* **2013**, *5* (19), 9522–9527. https://doi.org/10.1021/am402200n.

(42) Wang, H.; Wang, Z.; Yang, J.; Xu, C.; Zhang, Q.; Peng, Z. Ionic Gels and Their Applications in Stretchable Electronics. *Macromol. Rapid Commun.* **2018**, *39* (16), 1800246. https://doi.org/https://doi.org/10.1002/marc.201800246.

(43) Tao, X.; Stuart, B. W.; Wan, K.; Murray, J. W.; Bilotti, E.; Assender, H. E. Static and Dynamic Postannealing Strategies for Roll-to-Roll Fabrication of DC Magnetron Sputtered Bismuth Telluride Thin Films onto Polymer Webs. *ACS Appl. Mater. Interfaces* **2021**, *13* (8), 10149–10160. https://doi.org/10.1021/acsami.1c00721.

(44) Karakaya, M.; Zhu, J.; Raghavendra, A. J.; Podila, R.; Parler Jr., S. G.; Kaplan, J. P.; Rao, A. M. Roll-to-Roll Production of Spray Coated N-Doped Carbon Nanotube Electrodes for Supercapacitors. *Appl. Phys. Lett.* **2014**, *105* (26), 263103. https://doi.org/10.1063/1.4905153.

(45) Francis, G.; Stuart, B. W.; Assender, H. E. Selective Ozone Treatment of PDMS Printing Stamps for Selective Ag Metallization: A New Approach to Improving Resolution in Patterned Flexible/Stretchable Electronics. *J. Colloid Interface Sci.* **2020**, *568*, 273–281. https://doi.org/https://doi.org/10.1016/j.jcis.2020.02.008.

(46) Stuart, B. W.; Tao, X.; Gregory, D.; Assender, H. E. Roll-to-Roll Patterning of Al/Cu/Ag Electrodes on Flexible Poly(Ethylene Terephthalate) by Oil Masking: A Comparison of Thermal Evaporation and Magnetron Sputtering. *Appl. Surf. Sci.* **2020**, *505*, 144294. https://doi.org/https://doi.org/10.1016/j.apsusc.2019.144294.

(47) Tamagaki, H.; Ikari, Y.; Ohba, N. Roll-to-Roll Sputter Deposition on Flexible Glass Substrates. *Surf. Coatings Technol.* **2014**, *241*, 138–141. https://doi.org/https://doi.org/10.1016/j.surfcoat.2013.10.056.

(48) Kim, S. H.; Kim, C. H.; Choi, W. J.; Lee, T. G.; Cho, S. K.; Yang, Y. S.; Lee, J. H.; Lee, S.-J. Fluorocarbon Thin Films Fabricated Using Carbon Nanotube/Polytetrafluoroethylene Composite Polymer Targets via Mid-Frequency Sputtering. *Sci. Rep.* **2017**, *7* (1), 1451. https://doi.org/10.1038/s41598-017-01472-2.

(49) Raut, N. C.; Al-Shamery, K. Inkjet Printing Metals on Flexible Materials for Plastic and Paper Electronics. *J. Mater. Chem. C* **2018**, *6* (7), 1618–1641. https://doi.org/10.1039/C7TC04804A.

(50) Mathies, F.; List-Kratochvil, E. J. W.; Unger, E. L. Advances in Inkjet-Printed Metal Halide Perovskite Photovoltaic and Optoelectronic Devices. *Energy Technol.* **2020**, *8* (4), 1900991. https://doi.org/https://doi.org/10.1002/ente.201900991.

(51) Scholz, A.; Zimmermann, L.; Gengenbach, U.; Koker, L.; Chen, Z.; Hahn, H.; Sikora, A.; Tahoori, M. B.; Aghassi-Hagmann, J. Hybrid Low-Voltage Physical Unclonable Function Based on Inkjet-Printed Metal-Oxide Transistors. *Nat. Commun.* **2020**, *11* (1), 5543. https://doi.org/10.1038/s41467-020-19324-5.

(52) Silvestri, A.; Criado, A.; Poletti, F.; Wang, F.; Fanjul-Bolado, P.; González-García, M. B.; García-Astrain, C.; Liz-Marzán, L. M.; Feng, X.; Zanardi, C.; Prato, M. Bioresponsive, Electroactive, and Inkjet-Printable Graphene-Based Inks. *Adv. Funct. Mater.* **2022**, *32* (2), 2105028. https://doi.org/https://doi.org/10.1002/adfm.202105028.

(53) Soum, V.; Park, S.; Brilian, A. I.; Kim, Y.; Ryu, M. Y.; Brazell, T.; Burpo, F. J.; Parker, K. K.; Kwon, O.-S.; Shin, K. Inkjet-Printed Carbon Nanotubes for Fabricating a Spoof Fingerprint on Paper. *ACS Omega* **2019**, *4* (5), 8626–8631. https://doi.org/10.1021/acsomega.9b00936.

(54) Ardagh, M. A.; Birol, T.; Zhang, Q.; Abdelrahman, O. A.; Dauenhauer, P. J. Catalytic Resonance Theory: SuperVolcanoes, Catalytic Molecular Pumps, and Oscillatory Steady State. *Catal. Sci. Technol.* **2019**, *9* (18), 5058–5076. https://doi.org/10.1039/c9cy01543d.